A Parametric Method to Resolve the Ill-Posed Nature of the EIT Reconstruction Problem

A Simulation Study

J. C. DE MUNCK,[a] TH. J. C. FAES,[a] A. J. HERMANS,[b] AND R. M. HEETHAAR[a]

[a]*Laboratory of Clinical Physics and Informatics, Institute of Cardiovascular Research ICaR-VU, University Hospital Vrije Universiteit, 1007 MB Amsterdam, the Netherlands*

[b]*Section of Applied Mathematics, Faculty of Information Technology and Systems, Delft University of Technology, Delft, the Netherlands*

ABSTRACT: The reconstruction problem of electrical impedance tomography (EIT) is to estimate the distribution of the conductivity inside an object from measured potential distributions on the circumference caused by injected current patterns. Mathematically, this reconstruction problem is an ill-posed nonlinear inverse problem, with many unknowns. In this paper, the ill-posed nature is demonstrated by analyzing the condition of the sensitivity matrix; the associated inverse problem can only be solved on a very coarse grid. To circumvent the ill-posed nature of the EIT reconstruction problem, we present a new parametric formulation. In this formulation, it is assumed that the object consists of compartments with homogeneous conductivity. The position, orientation, size, and conductivity of these compartments are treated as unknown parameters, which are determined by solving the forward problem (using the boundary element method) and optimizing the parameters (using Powell's or the simplex method) in order to fit the parameters to the EIT data. Simulations show that the parametric method is stable and adequately solves the EIT problem.

INTRODUCTION

Electrical impedance tomography (EIT) is a technique to derive the distribution of the conductivity inside an object by injecting electric currents into the object and measuring the resulting potential distributions. This technique has applications in geophysics,[1,2] industry,[3] and biomedical engineering.[4] From a mathematical point of view, the EIT reconstruction problem is a rather difficult one. It is a *nonlinear, ill-posed* inverse problem with *many unknowns*. In a 2D image, the number of unknowns equals the number of pixels of the EIT image, typically on the order of 100 to 400.

Various EIT reconstruction techniques have been proposed and applied in the literature.[5] There is the more or less heuristic approach of Barber and Brown,[6,7] which was later given a firm mathematical basis in reference 8. This algorithm is very fast, but it is restricted to objects with a circular geometry. Another class of solution methods is based on an iterative application of the finite element method (FEM).[9] Here, the FEM is used to solve the forward problem (predicting the potentials for a given conductor geometry), and the differences between the predicted and measured potentials are minimized using a Newton-like algorithm. This "brute force" approach can be applied without a priori restrictions on the geometry, but is very time-consuming.

A completely different approach is to linearize the nonlinear problem, starting from a homogeneous conductor.[10] In this approach, the dependence of the measured potential distribution on the unknown impedance distribution is approximated by using a series expansion that is truncated at linear order. In this way, conductivity corrections to the homogeneous approximation can be found by solving a linear system of equations. The corresponding system matrix is usually called the *sensitivity matrix*. In the first part of this paper, we investigate the practical usefulness of this method by analyzing the condition of the sensitivity matrix for different discretizations of the conductivity.[11]

In the second part of the paper, we present a new formulation of the EIT reconstruction problem. Instead of trying to reconstruct the individual pixels of the image, we put as a priori information into the model that the object consists of compartments with constant (homogeneous) conductivity. The sizes, positions, and orientations of these compartments are treated as unknown parameters, whose values have to be estimated from the data using a parameter fitting procedure. The model predictions, that is, the computed potentials for a given conductor geometry, can be efficiently obtained using the boundary element method.[12] Simulations with our parametric formulation show that the EIT reconstruction problem transforms from an ill-posed nonlinear problem with many unknowns into a stable nonlinear parameter estimation problem with only a few unknowns.

THE SENSITIVITY MATRIX METHOD

The core equation of EIT, which describes the relationship between the conductivity $\sigma(\mathbf{x})$, the potential ψ, and the applied current density j, is here stated as

$$\begin{cases} \nabla \cdot (\sigma \nabla \psi) = 0, & \mathbf{x} \in \Omega \\ \sigma \nabla \psi \cdot \hat{\mathbf{n}} = j, & \mathbf{x} \in \partial\Omega. \end{cases} \tag{1}$$

Here, Ω represents a 2D cross section of the object, $\partial\Omega$ represents its circumference, and $\hat{\mathbf{n}}$ represents its outside normal. The current j is assumed to be zero, except at two points representing the injection electrodes. In this paper, we only consider the 2D version of the EIT problem. Therefore, we ignore the fact that, in practice, the currents may flow in three dimensions.

When ψ_A and ψ_B are two solutions of equation 1 with boundary conditions, j_A and j_B, the following identity can be derived:[13]

$$U_{AB} I_B = \int_{\Omega} \sigma \nabla \psi_A \cdot \nabla \psi_B d\Omega. \tag{2}$$

Here, I_B is the total current flowing through electrode pair B. Furthermore, U_{AB} is the potential difference measured by electrode pair B caused by a current injection of I_A through electrode pair A. In other words, U_{AB} is identical to the potential $\psi_A(\mathbf{x})$ evaluated at electrode pair B.

In a perturbation analysis, the conductivity and the potentials are expanded as follows:

(3)

$$\begin{cases} \sigma(\mathbf{x}) = \sigma^{(0)} + \sigma^{(1)}(\mathbf{x}) + \sigma^{(2)}(\mathbf{x}) + \dots \\ \psi_A(\mathbf{x}) = \psi_A^{(0)}(\mathbf{x}) + \psi_A^{(1)}(\mathbf{x}) + \psi_A^{(2)}(\mathbf{x}) + \dots \\ U_{AB} = U_{AB}^{(0)} + U_{AB}^{(1)} + U_{AB}^{(2)} + \dots \\ \psi_B(\mathbf{x}) = \psi_B^{(0)}(\mathbf{x}) + \psi_B^{(1)}(\mathbf{x}) + \psi_B^{(2)}(\mathbf{x}) + \dots \end{cases}$$

It is assumed that these series converge rapidly, so higher order terms are significantly smaller than lower order terms. Furthermore, it is assumed that $\sigma^{(0)}$ is constant in Ω. When the series expansions of equation 3 are substituted into equation 2 and terms of equal order in U_{AB} are collected, one finds after some manipulations (of which the details are described in a forthcoming paper[14]) that

$$U_{AB}^{(0)} I_B = \int_\Omega \sigma^{(0)} \nabla \psi_A^{(0)} \cdot \nabla \psi_B^{(0)} d\Omega \tag{4}$$

and

$$U_{AB}^{(1)} I_B = -\int_\Omega \sigma^{(1)} \nabla \psi_A^{(0)} \cdot \nabla \psi_B^{(0)} d\Omega. \tag{5}$$

When the potential is approximated to first order, that is, $U_{AB} \cong U_{AB}^{(0)} + U_{AB}^{(1)}$, the following linear relation between the measured potentials and the conductivity correction $\delta\sigma \equiv \sigma^{(0)} - \sigma^{(1)}$ is found:

$$U_{AB} \cong \frac{\int_\Omega \delta\sigma \nabla \psi_A^{(0)} \cdot \nabla \psi_B^{(0)} d\Omega}{I_B}. \tag{6}$$

In the reconstruction algorithm, this equation will be applied as follows. First, an initial guess $\sigma^{(0)}$ of the conductivity distribution is made. Using this guess, the potentials $\psi_A^{(0)}(\mathbf{x})$ and $\psi_B^{(0)}(\mathbf{x})$ are computed. Then, equation 6 gives a linear integral relationship between the measured potentials U_{AB} and the correction $\delta\sigma(\mathbf{x})$ of the initial guess $\sigma^{(0)}$. Since the measurements U_{AB} form a discrete set, the correction $\delta\sigma(\mathbf{x})$ has to be discretized too. This discretization is obtained by expanding $\delta\sigma(\mathbf{x})$ in a set of hat-shaped base functions $h_n(\mathbf{x})$, derived from a triangular grid (see FIGURE 1):

$$\delta\sigma(\mathbf{x}) \cong \sum_{n=0}^{N-1} \delta\sigma_n h_n(\mathbf{x}). \tag{7}$$

In this way, a piecewise linear approximation of the conductivity distribution is obtained, with $\delta\sigma = \delta\sigma_n$ on the n-th node. When the indices A and B, representing the applied current and voltage pairs, run over all noncoinciding and independent electrode pairs, equations 6 and 7 transform into a linear system of equations with the $\delta\sigma_n$ as unknowns:

$$U_k = \sum_{n=0}^{N-1} S_{kn} \delta\sigma_n, \quad k = 0, \dots, K-1. \tag{8}$$

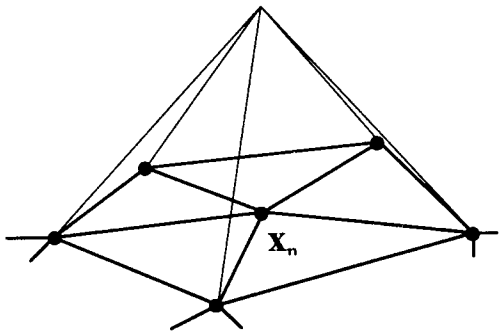

FIGURE 1. The discretization of the conductivity profile is obtained by expanding the conductivity in a series of hat-shaped functions, which are derived from a triangular grid. Here, the base function $h_n(\mathbf{x})$ is shown, which equals 1 at node $\mathbf{x}_n$ and falls off linearly to zero at the neighboring nodes.

Here, the combinations of A and B are referred to by the index k. The matrix S_{kn} is the so-called *sensitivity matrix*, which can be expressed as

$$S_{kn} \equiv \frac{\int_\Omega h_n(\mathbf{x}) \nabla \psi_A^{(0)}(\mathbf{x}) \cdot \nabla \psi_B^{(0)}(\mathbf{x}) d\Omega}{I_B}. \tag{9}$$

In theory, the number of discretization points N can be chosen equal to the number of independent measurements. In the case that neighboring electrodes are used, this number is $K \equiv (1/2)N_e(N_e - 3)$, with N_e being the number of electrodes. In FIGURE 2A, a discretization is shown, with $N_e = 16$ electrodes and $K = 104$ nodes. However, in practice, the number of discretization points that can be reconstructed may be much smaller because many of the equations in equation 8 may be (almost) linearly dependent. When this is the case, the solution of equation 8 becomes unstable and highly sensitive to modeling errors and to noise in the measurements. The problem can be simply solved by taking less discretization points than the number of independent measurements ($N < K$) and finding the least-squares solution of the overdetermined system of equations. In FIGURES 2B and 2C, such discretizations are depicted, with $N = 48$ and $N = 28$ nodes.

A least-squares solution can be found by performing a singular value decomposition (SVD) on the matrix S:[15]

$$S_{kn} = \sum_{i=0}^{N-1} \lambda_i \mathbf{u}_i \mathbf{v}_i^T, \quad \text{with} \quad \lambda_0 \geq \lambda_1 \geq \lambda_2 \geq \ldots \geq \lambda_{N-1} \geq 0, \tag{10}$$

where the sets of vectors $\mathbf{u}_i$ and $\mathbf{v}_i$ are the orthonormal sets of dimensions K and N, respectively. When N is chosen so small that all singular values λ_i are positive, the least-squares solution of equation 7 can be expressed as

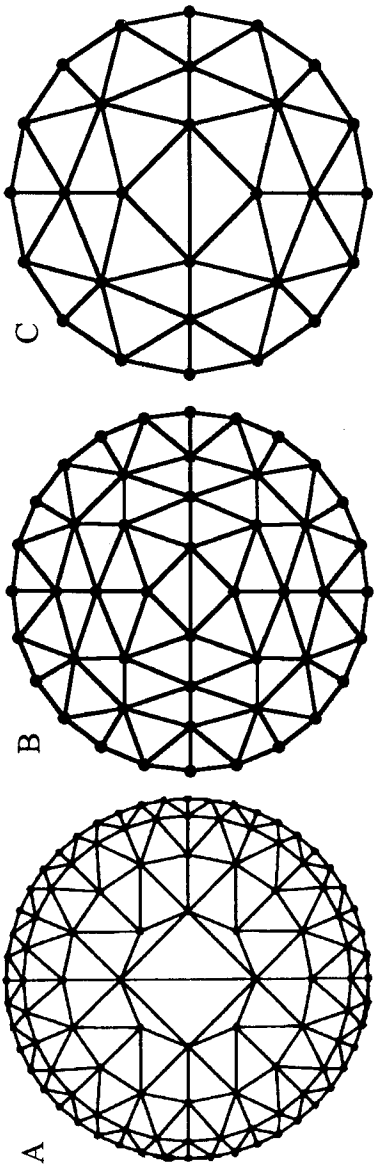

FIGURE 2. (A) An example of a grid on which the conductivity distribution is discretized. Here, the number of electrodes is 16. The number of discretization points N is maximum (104). The number of discretization points is reduced to 48 in part B and to 28 in part C.

$$\delta\sigma = \sum_{i=0}^{N-1} \frac{(\mathbf{u}_i^T \mathbf{U})}{\lambda_i} \mathbf{v}_i \tag{11}$$

where $\delta\sigma$ and $\mathbf{U}$ represent the vectors of the unknowns and the measurements, respectively. Equation 11 nicely demonstrates the instability of the solution when the equations become almost linearly dependent. In that case, the smallest singular values tend to zero and blow up the reconstruction when $\mathbf{U}$ contains measurement errors.

RESULTS: THE SENSITIVITY MATRIX

To investigate the practical possibilities of the sensitivity matrix method, we assumed that the object had a circular shape. In this case, the potentials $\psi_A^{(0)}$ and $\psi_B^{(0)}$ can be computed analytically. However, the integrations in equation 9 have to be performed numerically. We furthermore assumed that all currents are injected through neighboring electrodes and that they are equal in magnitude. Finally, it is assumed that the potentials are also measured by neighboring electrodes and that the number of electrodes equals 16. For this case, the sensitivity matrix (equation 9), its singular values (equation 10), and its conductivity distribution (equation 11) were computed.

FIGURE 3 shows the singular values as a function of the index i. Obviously, the singular values range over 16 orders of magnitude, indicating the instability of the solution of the inverse problem. One way to deal with this problem is to smooth the inverse solution by truncating the series in equation 11 or to add a positive constant to all λ_i terms. However, the quality of the inverse solution so obtained is highly dependent on the exact way that the smoothing is obtained (e.g., see reference 11). Therefore, we choose to reduce the number of unknowns instead, using the grids depicted in FIGURES 2B and 2C.

To demonstrate the performance of the method, we show here the result of a simulation study. A set of measurements was simulated by assuming a circular conductor with conductivity 1 (in arbitrary units) and two circular holes with conductivities 0.9 and 0.8; see FIGURE 4. The conductivities were chosen close to 1 because only then we may assume that the series in equation 3 will converge fast enough.

For the initial guess, the correct value of 1 was chosen. The sensitivity matrix was determined and the conductivity distribution was estimated using equation 11. FIGURE 5 shows the results on a grid of 48 points (A) and on a grid of 28 points (B). It appears that the main characteristics of the true impedance image are well estimated. However, the sizes of the smaller circles are hard to estimate from the reconstructed images. Other simulations, not shown here, also demonstrate that the main characteristics are estimated well with both the 48- and 28-point grids.

Our conclusion about the sensitivity method is that, when no noise is present, it is capable of reconstructing the low spatial frequencies, but only when the reconstruction is performed on a coarse grid. Detailed information of the object cannot be retrieved. Although, in principle, the number of pixels that can be reconstructed equals $(1/2)N_e(N_e - 3)$, in practice this upper bound is far too optimistic. Furthermore, the method is based on the assumptions that a good first guess of $\sigma^{(0)}$ is available and that the true conductivity distribution does not deviate too much from this constant.

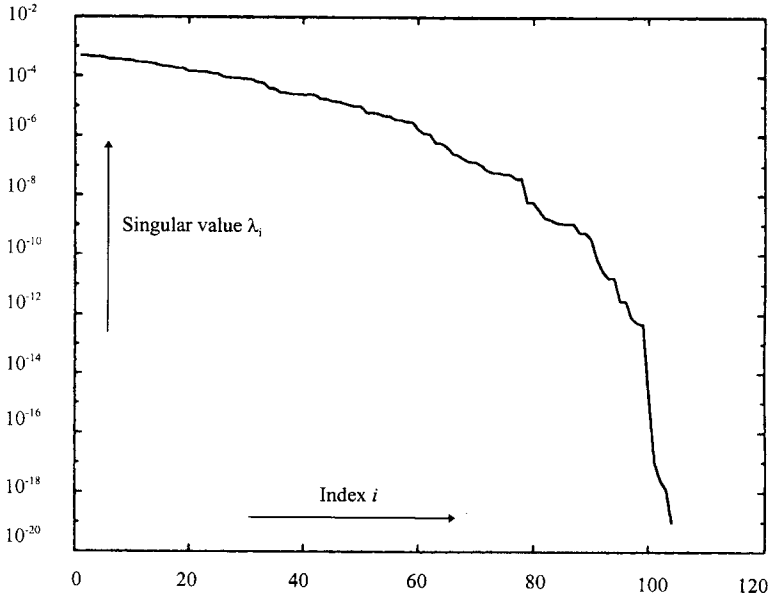

FIGURE 3. The distribution of the singular values of the sensitivity matrix S for the case of a circular cross section with 16 electrodes attached to the circumference. It follows that the singular values are within a range of 16 orders of magnitude, indicating that the full system of equations contains many linear dependencies and hence that the reconstruction is highly unstable.

THE PARAMETRIC METHOD

To overcome the difficulties of the sensitivity matrix method, we propose a reconstruction method in which the number of parameters that have to be estimated is limited and in which no linearization assumptions are required. In this proposed method, we assume that the object consists of compartments with constant conductivity, with unknown positions, orientations, sizes, and conductivities. With such a method, it is also very simple to use a priori information in the reconstruction, by simply setting some parameters to a known constant. The inverse problem is to determine that set of parameters giving the best description of the measurements.

For the application of the parametric method, two problems have to be solved—the forward and the inverse problem. The forward problem is to determine the potential distribution at the measuring electrode for a given set of current injection electrodes and a given conductor geometry. The inverse problem—the geometry of the conductor—is adapted iteratively in such a way that the deviation between the measured and the predicted potentials is minimum. Since we assume a piecewise constant conductivity profile, we can use the boundary element method (BEM)[12] in the forward computations. The BEM is based on the discretization of an integral equation that gives an implicit relationship between the potentials on the surfaces of a conductor with a piecewise constant conductivity. When a current density $j_0(\mathbf{x})$ is injected into the surface Γ_0 of an isolated 2D conductor (FIGURE 6),

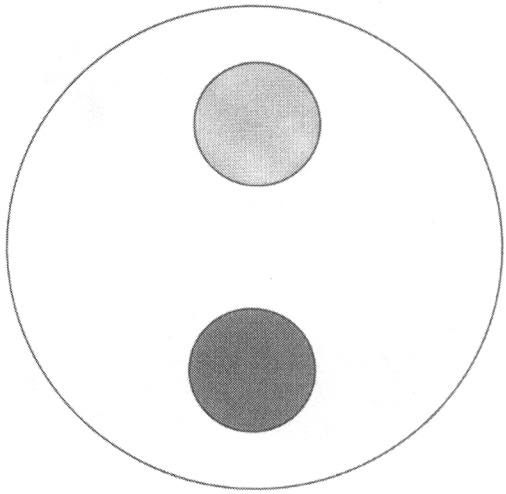

FIGURE 4. The conductor used for the simulation study to test the performance of the sensitivity method. The conductivity equals 1 (in arbitrary units), except at two circular parts. The conductivity of the upper circle equals 0.9, whereas the conductivity of the lower circle equals 0.8.

which consists of a set of J nested contours Γ_j ($j = 0, \ldots, J-1$) with inner conductivity σ_j^- and outer conductivity σ_j^+, the following system of integral equations is valid for the potential $\psi(\mathbf{x})$ on the contours:

$$\pi[\omega^-(\mathbf{x}) + \omega^+(\mathbf{x})]\psi(\mathbf{x}) = \oint_{\Gamma_0} \log(R^{-1}) j_0 d\gamma' + \sum_{j=0}^{J-1} (\sigma_k^- - \sigma_k^+) \oint_{\Gamma_j} \psi \nabla' \log(R^{-1}) \otimes d\gamma \quad (12)$$

where $R \equiv |\mathbf{x} - \mathbf{x}'|$, $\mathbf{x} \in \Gamma_k$, and $k = 0, \ldots, J-1$.

Here, ∇' is the gradient operator with respect to the integration point $\mathbf{x}'$, $d\gamma'$ is a line element along the contour, and the operator $\otimes$ yields the determinant of the vectors $\nabla' \log(R^{-1})$ and $d\gamma'$. Equation 12 can be obtained in a way very similar to reference 16, where an integral equation for the potential distribution caused by a current source inside a piecewise constant conductor is derived. Instead of the infinite medium potential that appears in references 12 and 16, we here have the first integral on the right-hand side playing the role of the source term.

Equation 12 can be discretized by expanding the potential in a set of hat-shaped base functions $h_n(\mathbf{x})$,

$$\psi(\mathbf{x}) \cong \sum_{n=0}^{N-1} \psi_n h_n(\mathbf{x}), \quad (13)$$

and subdividing the contours into a set of segments ranging from $\mathbf{x}_0$ to $\mathbf{x}_1$, $\mathbf{x}_1$ to $\mathbf{x}_2$, . . . ,$\mathbf{x}_{N-2}$ to $\mathbf{x}_{N-1}$. The base functions are chosen such that they equal 1 at the point $\mathbf{x}_n$ and linearly fall off to zero for points before and after the point $\mathbf{x}_n$ (FIGURE 7).

FIGURE 5. The reconstructed conductivity distribution using the sensitivity method. As input, the potentials simulated with the conductor of FIGURE 4 were used: (A) reconstruction on a grid of 48 points; (B) reconstruction on a grid of 28 points.

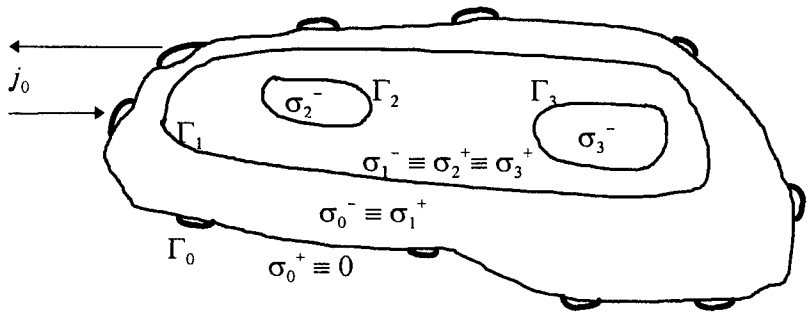

FIGURE 6. Graphical presentation of the geometry of the problem and the meaning of the symbols. The outer conductivity of a contour is the inner conductivity of another contour. In the example presented here, we have $\sigma_1^- \equiv \sigma_2^+ \equiv \sigma_3^+$ and $\sigma_0^- \equiv \sigma_1^+$. The conductor is completely characterized by the shapes of the contours and their inner conductivities.

Similar to the derivation of the system of equations in the sensitivity matrix method, we obtain a linear system of equations when equation 13 is substituted into equation 12:

$$\sum_{n=0}^{N-1} a_{mn}\psi_n = b_m \tag{14}$$

where the matrix elements a_{mn} and the right-hand side b_m can be computed analytically.[17] The system itself can be solved using a standard LU decomposition. By nature of the boundary element method and contrary to the sensitivity matrix method, the potential at the boundaries is discretized instead of the (unknown) conductivity inside the complete object. Therefore, in both discretizations, different types of base functions are involved.

The inverse problem is to find that combination of parameters for which the difference between the measured and predicted is minimum. This difference can be expressed in the cost function E:

$$E = \sum_A \frac{\sum_B |\tilde{U}_{AB} - U_{AB}|}{\sum_B |U_{AB}|} \cdot 100\% \tag{15}$$

where U_{AB} denotes the measured potential difference on electrode pair B caused by a current injection on electrode pair A, and $\tilde{U}_{AB}$ denotes the corresponding model prediction. The index A runs over all pairs of current injection electrodes that are used in the data acquisition and B runs over all voltage-measuring electrode pairs, except those that coincide with one of the current injection electrodes.

The predicted potentials $\tilde{U}_{AB}$ depend on the positions, shapes, and inner conductivities of the contours representing the conductor. In the inverse algorithm that we are proposing, a conductor is chosen as a starting value and next the contours are shifted, rotated, and stretched,

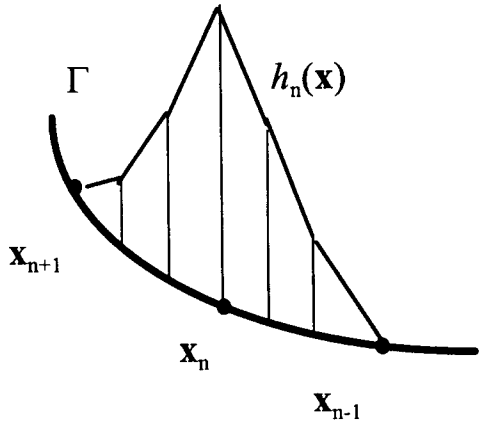

FIGURE 7. The base functions used to expand the potential. These functions are defined for **x** on a contour. They equal unity at one of the vertices and gradually fall off to zero at the next and the previous vertex on the contour.

$$\begin{pmatrix} \xi' \\ \eta' \end{pmatrix} = \begin{pmatrix} s\cos\varphi & -s\sin\varphi \\ s\sin\varphi & s\cos\varphi \end{pmatrix} \begin{pmatrix} \xi \\ \eta \end{pmatrix} + \begin{pmatrix} t_\xi \\ t_\eta \end{pmatrix}, \tag{16}$$

in order to minimize the cost function. Here $(t_\xi, t_\eta)^T$ is the translation vector, φ is the rotation angle, and s is the stretching parameter. These transformations are separately applied for each contour. With this parameterization, there are four unknowns per contour, excluding the inner conductivity.

The minimization of the cost function is a nonlinear problem that can only be solved by iterative methods. For a proper functioning of nonlinear minimization methods, the parameters should be scaled such that a fixed step in each of the scaled parameters roughly has the same effect on the cost function. Furthermore, the parameters s and σ^- are kept positive by optimizing their logarithms. Each time that the minimization algorithm computes the next step, it uses the scaled parameters; and each time that this algorithm requires a cost function evaluation, the parameters are transformed back into their unscaled versions. We used either the simplex method or Powell's method[15] to minimize the cost function.

RESULTS: THE PARAMETRIC METHOD

To test the efficiency and robustness of our proposed inverse algorithm, we used a standard conductor shown in FIGURE 8. This conductor has a conductivity $\sigma^- = 1$, and it contains two large structures with a low conductivity ($\sigma^- = 0.1$) and a small good-conducting structure ($\sigma^- = 10$). Because of the resemblance between the standard geometry and the 2D cross section of the torso, the inner structures of the conductor will hereafter be referred to as lungs and aorta. It is assumed that the standard conductor has 32 equally spaced electrodes mounted on its outer contour.

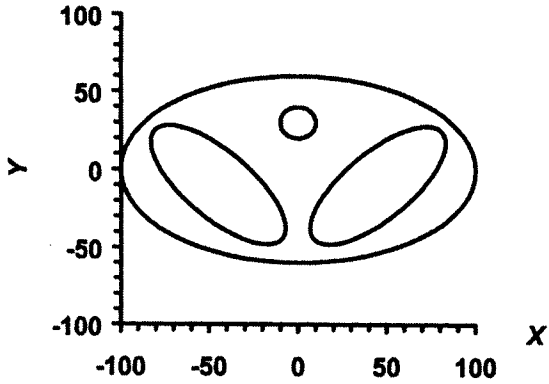

FIGURE 8. "Standard" conductor from which simulations are performed. The outer ellipse has a conductivity of $\sigma^- = 1$, the two big elliptical structures are relatively poor conducting ($\sigma^- = 0.1$), and the small circle is good conducting ($\sigma^- = 10$).

We studied the behavior of the simplex and Powell's minimization algorithms. In a simulation study, the standard geometry was distorted by moving, rotating, and scaling the lungs and keeping the other contours constant. Twenty-five random distortions were applied and, for each of these distortions, it was attempted to find back the standard geometry using the distorted geometry as a starting value and the potentials U_{AB} of the standard geometry as simulated data. The *success rate* and the number of BEM evaluations were determined. The success rate is defined as the relative number of reconstructions, for which the *average distance* between the standard conductor and the reconstructed conductor is less than 1% of the conductor's diameter. Here, the average distance is computed by averaging all distances between corresponding points (of the free contours). The number of BEM evaluations is proportional to the total computation time of the inverse algorithm.

It appears from TABLE 1 that the success rate of Powell's algorithm is 88% and that for the simplex method is 100%. The number of BEM evaluations is of the same order of magnitude.

TABLE 1. A Comparison of the Performance between the (Modified) Simplex and Powell's Minimization Method

Minimization Method	Success Rate	Number of BEM Evaluations
Powell's	88%	820
Simplex	100%	1024

DISCUSSION

Comparing the sensitivity matrix method and the parametric method from a theoretical point of view, we note that the applicability of the parametric method is much less restricted. With the sensitivity matrix method, a first guess of the conductivity is required, from which the true conductivity distribution must not deviate too much. Otherwise, the linear approximation becomes invalid. One could attempt to circumvent this disadvantage by deriving higher order approximations or by starting from an inhomogeneous distribution $\sigma^{(0)}(\mathbf{x})$ as a first guess. However, whether such variants would yield practical reconstruction methods is questionable because the derivation of equation 6 is based on the assumption that $\sigma^{(0)}$ is constant.

One could object that the comparison between both methods is not fair because the number of electrodes was 32 in the simulations with the parametric method and this number was only 16 with the sensitivity matrix method. Moreover, the number of unknowns was 8 with the parametric method and it was minimally 28 with the sensitivity matrix method. The reason why we used only 16 electrodes with the sensitivity matrix method is that, because of the piecewise linear approximation of the conductivity, with a larger number of electrodes, more triangles would have to be chosen at the boundary. This would decrease the resolution at the center still further. Furthermore, we consider the fact that the number of unknowns in the parametric method was only 8 as a special advantage of this method. With the sensitivity matrix method, the use of a grid with 8 nodes would have no practical meaning because the resolution would be too low.

The main theoretical restriction of the parametric method is the assumption that the object consists of nested compartments with constant conductivity. In principle, one could avoid this restriction by taking a sufficient number of small compartments. Practical limitations of this approach are that the method could become unstable and that the computation time would increase enormously. With the simulations presented in the previous section, where the number of compartments is limited, on average 1000 BEM evaluations were required, taking about 30 minutes on a fast PC.

Currently, the computation time is the main drawback of the parametric method. There are various possibilities to speed up the algorithm. First, one could use iterative methods to solve equation 14 instead of a full LU decomposition. Good initial guesses are available from previous cost function evaluations. Second, one could use the method described in reference 18 to solve a series of boundary element problems, in which only one or two compartments are different. Third, one could investigate whether our modifications of the simplex and Powell's method could be improved. However, we do not expect that these improvements will ever make the parametric method faster than the sensitivity matrix method, where each image reconstruction only requires a simple matrix vector multiplication.

The parametric method and the sensitivity matrix method also differ in the way that a priori knowledge is used in the reconstruction and in the amount of a priori knowledge used. For this reason, we will continue to explore both methods not only from a theoretical point of view, but also from a clinical point of view. In some cases, where one is interested in extracting detailed physical quantities from the data, and sufficient a priori information is available, the parametric method would be the most favorable algorithm. In other cases, where one is interested in fast changes in gross anatomy, the sensitivity matrix method is the method of choice.

ACKNOWLEDGMENTS

The part of this paper dealing with the sensitivity matrix is based on the master's thesis of Ir. L. Riemens. We wish to thank her for all the work she did.

REFERENCES

1. CHERKAEVA, E. & A.C. TRIPP. 1996. Inverse conductivity problem for inaccurate measurements. Inverse Probl. **12:** 869–883.
2. BORCEA, L., J.G. BERRYMAN & G.C. PAPANICOLAOU. 1996. High-contrast impedance tomography. Inverse Probl. **12:** 835–858.
3. PLASKOWSKI, A., M.S. BEEK, R. THORN & J. PYAKOWSKI. 1995. Imaging Industrial Flows: Applications of Electrical Process Tomography. Inst. Phys. Pub. Bristol/Philadelphia.
4. BROWN, B.H., D.C. BARBER & A.D. SEAGAR. 1985. Applied potential tomography: possible clinical application. Clin. Phys. Physiol. Meas. **6:** 109–121.
5. WEBSTER, J.G., Ed. 1990. Electrical Impedance Tomography. Adam Hilger. Bristol/New York.
6. BARBER, D.C. & B.H. BROWN. 1984. Applied potential tomography. J. Phys. E. Sci. Instrum. **37:** 723–732.
7. BARBER, D.C. & A.D. SEAGAR. 1987. Fast reconstruction of resistance images. Clin. Phys. Physiol. Meas. **8**(suppl. A): 47–54.
8. SANTOSA, F. & M. VOGELIUS. 1990. A backprojection algorithm for electrical impedance imaging. SIAM J. Appl. Math. **50:** 216–243.
9. YORKEY, T.J., J.G. WEBSTER & W.J. TOMPKINS. 1987. Comparing reconstruction algorithms for electrical impedance tomography. IEEE Trans. Biomed. Eng. **BME-34:** 843–851.
10. CALDERON, A.P. 1980. On an inverse boundary value problem. Seminar on Numerical Analysis and Its Application to Continuum Mechanics (Soc. Brasileira de Mathematica, Rio de Janeiro), p. 65–73.
11. DE MUNCK, J.C. 1997. A comparison of methods to determine mass transports from hydrographic measurements. J. Phys. Oceanogr. **27:** 1635–1653.
12. DE MUNCK, J.C. 1992. A linear discretization of the volume conductor boundary integral equation using analytically integrated elements. IEEE Trans. Biomed. Eng. **BME-39:** 986–989.
13. BRECKON, W.R. & M.K. PIDCOCK. 1987. Mathematical aspects of impedance imaging. Clin. Phys. Physiol. Meas. **8**(suppl. A): 77–84.
14. FAES, TH. J.C. *et al.* 1998. In preparation.
15. PRESS, W.H., B.P. FLANNERY, S.A. TEUKOLSKY & W.T. VETTERLING. 1988. Numerical Recipes in C. Cambridge University Press. London/New York.
16. BARNARD, A.C.L., J.M. DUCK, M.S. LYNN & W.P. TIMLAKE. 1967. The application of electromagnetic theory to electrocardiology II. Biophys. J. **7:** 463–491.
17. DE MUNCK, J.C., TH. J.C. FAES & R.M. HEETHAAR. 1998. The use of the boundary element method in electrical impedance tomography. *In* Boundary Element Research in Europe, p. 115–125. Computational Mechanics Pub. Southampton.
18. LOBRY, J. 1998. A new fast method for solving problems with moving boundary. *In* Boundary Element Research in Europe, p. 167–178. Computational Mechanics Pub. Southampton.